Electronic Supplementary Information (ESI) for

Water-soluble ruthenium complex-pyrene dyads with extended triplet lifetimes for efficient energy transfer applications

Arne C. Sell,[a] Julius C. Wetzel,[a] Matthias Schmitz,[a] A. Wouter Maijenburg,[b] Georg Woltersdorf,[c] Robert Naumann[a,b] and Christoph Kerzig*[a]

[a] Department of Chemistry, Johannes Gutenberg University Mainz, Duesbergweg 10—14, 55128 Mainz, Germany.

[b] Center for Innovation Competence SiLi-Nano, Martin-Luther-University Halle-Wittenberg, Karl-Freiherr-von-Fritsch-Straße 3, 06120 Halle, Germany.

[c] Institute of Physics, Martin-Luther-University Halle-Wittenberg, Von-Danckelmann-Platz 3, 06120 Halle, Germany.

Contents

S1 General experimental details and methods

Materials

Unless otherwise noted, all chemicals used for synthesis, optical spectroscopy and irradiation experiments were obtained commercially in high purity and used as received (acetone, ≥99.8%, fisher scientific; acetonitrile, ≥99.9%, VWR Chemicals; ammonium hexafluorophosphate, 99.5%, abcr; barium hydroxide octahydrate, ≥98%, Sigma-Aldrich; 5-bromo-1,10-phenanthroline, Fluorochem; chloroform, 99.5%, Titolchimica; *cis*-dichlorobis(2,2'-bipyridine)ruthenium(II), 97%, Sigma-Aldrich; dichlorobis(1,10-phenanthroline)ruthenium(II), still available from a former project[1]; dichloromethane, ≥99.9%, VWR Chemicals; *N,N*-dimethyl-4-nitrosoaniline, 98%, fisher scientific; disodium phosphate, ≥99%, Sigma-Aldrich; ethanol, ≥99.8, fisher scientific; hydrochloric acid, 37%, VWR Chemicals; 5-(hydroxymethyl)furfural, 98%, abcr; imidazole, >98%, TCI; maleic acid, >99%, TCI; methanol, ≥99.9%, VWR Chemicals; 9-(methylaminomethyl)anthracene, 99%, Sigma-Aldrich; 1-pyreneboronic acid, TCI; sodium chloride, ≥99.5%, fisher scientific; sodium dihydrogen phosphate monohydrate, ≥99%, Sigma-Aldrich; sodium hydroxide, ≥98%, Sigma-Aldrich; sodium sulfate, 99%, Acros Organics; sulfuric acid, 96%, Carl Roth; tetrakis(triphenylphosphine)palladium(0), 99.9%, fisher scientific; toluene, ≥99.8%, fisher scientific; triethylamine, ≥99%, VWR Chemicals; tris(2,2'-bipyridyl)-dichlororuthenium(II) hexahydrate, 99.95%, Sigma-Aldrich; tris(1,10-phenanthroline)-dichlororuthenium(II) hydrate, 98%, Sigma-Aldrich). Aqueous solutions were prepared using ultrapure Millipor MilliQ water with a specific resistance of 18.2 MΩ cm. Unless otherwise indicated, Argon from Nippon Gases (5.0) was used for removing dissolved oxygen prior to all synthetic reactions (20 min) and spectroscopic experiments (10–30 min). Cuvettes with septum caps were used for optical spectroscopy and sealed under argon (1 atm).

Steady-state measurements

Absorption measurements were carried out with a Perkin Elmer LAMBDA 365 instrument. Emission spectra were recorded using a Perkin Elmer FL-6500 spectrometer. All steady-state absorption and luminescence measurements were performed at room temperature (24 ± 2 °C) and very low concentrations of the emissive compounds were employed to avoid filter effects. The wavelength sensitivity correction for our emission instrument is reliable up to 660 nm. Hence, we do not show emission spectra above this wavelength.

Laser flash photolysis (LFP)

The LP980KS setup from Edinburgh Instruments equipped with both a Nd:YAG-laser from Litron (Nano LG 300-10) and a Nd:YAG-laser from Quantel (Q-smart 450) was employed for laser flash photolysis, either to record transient absorption or emission signals. The frequency-doubled (532 nm) output of

one of the lasers served as excitation source; the laser and its settings were not modified within a series of experiments. For both lasers, the pulse duration was about 10 ns and the pulse frequency was 10 Hz. The typical pulse energy used for transient absorption and emission studies was 30 mJ (Litron), while the excitation intensities of the Quantel laser were varied by modifying the Q-switch delays between 50 µs (~100 mJ) and 125 µs (~15 mJ). Beam expanders (Thorlabs) were used to ensure homogeneous excitation in the detection volume (beam diameter in front of the cuvette window, about 1.2 cm (Litron) and 0.8 cm (Quantel)), thus allowing the precise determination of excited state concentrations in the cuvette as well as reliable kinetic analyses. Detection of transient absorption spectra occurred on an iCCD camera from Andor. Single-wavelength kinetics were recorded using a photomultiplier tube from Hamamatsu (R928). The spectroscopic experiments were performed using a cuvette holder that allows temperature control. If not stated otherwise the LFP measurements were performed at 20 °C and the TA spectra were integrated over 100 ns.

LED irradiation experiments

Application-related irradiation experiments were conducted with a 525 nm LED (Kessil Science, PR160L). This light source has four power settings (25%, 50%, 75% and 100%) and the average intensity (at 100% output power) is reported as 352 mW cm^{-2} (measured from 1 cm distance).[2] An emission spectrum of the LED was measured by irradiating a water-containing cuvette in the FL-6500 instrument and recording the Rayleigh scattering light; the spectrum so obtained is shown in Fig. S19 (appendix). The light source was installed in a 90° angle with respect to the detector.

Chromatography

For standard liquid column chromatography separation, silica gel 60 M (0.040-0.063 mm Macherey-Nagel GmbH & Co., Düren, Germany) was used. Thin-layer-chromatography was performed using "DC Kieselgel 60 F254" (Merck KGaA, Darmstadt, Germany) on aluminum and a UV lamp (Herolab GmbH, NU-8, λ = 254 nm and 365 nm, Wiesloch, Germany) was employed for detection. The resulting R_f values are given relative to the solvent.

Anion exchange reactions of the PF_6 complexes to the chloride salts were carried out using *Amberlite IRA-410* (Sigma-Aldrich) in methanol or acetone. Before each ion exchange, the resin was regenerated several times with a 10 mM aqueous sodium chloride solution followed by rinsing with the respective solvent to remove unadsorbed ions.

NMR spectroscopy

NMR spectroscopic studies were performed on an Avance II 400 multi nuclear magnetic resonance spectrometer (Bruker, analytic measuring technique, Karlsruhe, Germany). The solvents used were chloroform-d_1, acetone-d_6, acetonitrile-d_4 or water-d_2 (Deutero GmbH, Kastellaun, Germany). The ^{1}H NMR spectra were calibrated using the residual non-deuterated solvent[3] and the chemical shifts are given as δ values in ppm. All coupling constants J are given in Hertz (Hz).

Mass spectrometry

Accurate mass determinations were made on a G6545A Q-ToF instrument (Agilent GmbH, Waldbronn, Germany) with electrospray ionization (ESI). Sample inlet was via a 1260 Infinity II HPLC system (Agilent GmbH, Waldbronn, Germany) with G7111B 1260 Quaternary Pump, G7129A 1260 Vialsampler, and G7116A 1260 Multicolumn Thermostat. Mass calibration was performed on the day of measurement using an external standard. The expected mass accuracy is better than 5 ppm for the measurements presented herein.

HPLC-measurements

Purity determination by HPLC was performed using an AS-2051Plus autosampler (JASCO Deutschland GmbH, Pfungstadt, Germany), two PU-2087Plus pumps (JASCO Deutschland GmbH, Pfungstadt, Germany), and a UV-2075Plus UV detector (JASCO Deutschland GmbH, Pfungstadt, Germany). Using a solvent gradient of water and acetonitrile, an injection volume of 10 µL was separated at a flow rate of 1 mL/min via a Reprosil 100 C18 5 µm column and analyzed at 254 nm and 450 nm with the UV-Vis detector.

DFT calculations

Quantum-mechanical calculations were carried out with the Gaussian 09 package[4] using the B3LYP functional in combination with the LANL2DZ basis set. Geometry optimizations and accompanied frequency analyses were performed with the ground states and lowest triplet states of both dyads. All optimized geometries used for further computations did not show imaginary vibrational frequencies, indicating convergence on minimum structures. The computed orbitals, orbital coefficients and spin densities mentioned in the main paper were obtained by additional single-point calculations with population analyses. The results of our DFT calculations were visualized (main paper, Fig. 3) with the software Avogadro.

S2 Synthetic procedures and characterization data

Unless stated otherwise, all air- or moisture-sensitive syntheses were performed under inert conditions (Ar atmosphere). Solutions of the target complexes were protected from light (during synthesis and purification), and the isolated products were stored in the dark.

S2.1 Synthesis of 5-(Pyren-1-yl)-1,10-phenanthroline (Py)

The ligand **Py** was prepared from 5-bromo-1,10-phenanthroline (0.98 g, 3.78 mmol) and pyrene-1-ylboronic acid (1.03 g, 4.19 mmol) in a two-phase mixture of toluene (160 mL), ethanol (52 mL) and an aqueous $Ba(OH)_2$ solution (208 mL) following the procedure previously reported by Castellano *et al.*[5] (refluxed under Ar atmosphere for two days). Half of the raw product obtained was subsequently purified by column chromatography (DCM/MeOH, 50:1 + one drop of NEt_3) to yield **Py** (0.31 g, 21%) as a yellowish solid.

^{1}H NMR data with acetone-d_6 as solvent are in agreement with those presented in the literature.[5]

R_f = 0.12 (DCM/MeOH, 50:1 + one drop of NEt_3).

ESI-HRMS: Calcd. for $C_{28}H_{17}N_2^+$ ($[M+H]^+$): m/z 381.1386, found: m/z 381.1379.

Calcd. for $C_{28}H_{16}N_2Na^+$ ($[M+Na]^+$): m/z 403.1206, found: m/z 403.1198.

^{1}H NMR (400 MHz, acetone-d_6) δ [ppm] = 9.22 (d, *J*=4.7, 1H), 9.15 (d, *J*=4.2, 1H), 8.55 (d, *J*=8.0, 1H), 8.48 (d, *J*=7.8, 1H), 8.38 (dd, *J*=7.7, 1.1, 1H), 8.35 – 8.25 (m, 3H), 8.18 (d, *J*=7.7, 1H), 8.15 – 8.08 (m, 2H), 8.05 (d, *J*=9.2, 1H), 7.84 (dd, *J*=8.1, 4.3, 1H), 7.77 (d, *J*=8.2, 1H), 7.70 (d, *J*=9.2, 1H), 7.56 (dd, *J*=8.3, 4.2, 1H).

^{1}H NMR (400 MHz, $CDCl_3$): δ [ppm] = 9.35 (dd, *J*=4.4, 1.7, 1H), 9.27 (dd, *J*=4.3, 1.7, 1H), 8.37 (dd, *J*=8.1, 1.7, 1H), 8.33 (d, *J*=7.8, 1H), 8.27 (dd, *J*=7.7, 1.2, 1H), 8.20 – 8.16 (m, 3H), 8.08 – 8.03 (m, 2H), 8.00 (s, 1H), 7.93 (d, *J*=9.2, 1H), 7.82 (dd, *J*=8.3, 1.7, 1H), 7.77 (dd, *J*=8.1, 4.5, 1H), 7.61 (d, *J*=9.2, 1H), 7.46 (dd, *J*=8.3, 4.3, 1H).

S2.2 Synthesis of Bis(2,2'-bipyridine)(5-pyrenyl-1,10-phenanthroline)ruthenium(II) chloride, $[Ru(bpy)_2(phenPy)]Cl_2$ (RubpyPy)

The sensitizer **RubpyPy** was prepared from *cis*-dichlorobis-(2,2'-bipyridine)ruthenium(II) (374 mg, 0.72 mmol) and **Py** (303 mg, 0.80 mmol) in methanol (300 mL) following the procedure previously reported by Castellano *et al.*[5] (refluxed under Ar for 3 h). After cooling to room temperature, water (100 mL) was added and the PF_6 salt (332 mg, 43%) was precipitated by dropwise addition of 50 mL saturated $NH_4PF_{6(aq)}$. 60 mg of the salt were purified by vapor diffusion technique ($MeCN/Et_2O$) and were subsequently converted to the chloride salt by anion exchange with *Amberlite IRA-410* (MeOH/MeCN, 10:1). After removing the solvents under reduced pressure, **RubpyPy** (40 mg, 6.4%) was obtained as a red solid.

R_f = 0.48 (acetone/H_2O/sat. aqueous NaCl 40:20:1).

ESI-HRMS: Calcd. for $C_{48}H_{32}ClN_6Ru^+$ ([M-Cl]$^+$): m/z 829.1415, found: m/z 829.1433.

Calcd. for $C_{48}H_{32}N_6Ru^{2+}$ ([M-2Cl]$^{2+}$): m/z 397.0860, found: m/z 397.0876.

^{1}H NMR (400 MHz, CD_3CN): δ [ppm] = 8.81 – 8.64 (m, 5H), 8.51 – 8.34 (m, 3H), 8.34 – 8.24 (m, 3H), 8.24 – 7.66 (m, 15H), 7.66 – 7.59 (m, 1H), 7.53 – 7.44 (m, 3H), 7.44 – 7.37 (m, 1H), 7.35 – 7.28 (m, 1H).

HPLC (gradient with water 100% to acetonitrile 100%): purity at 254 nm 98.0%; purity at 450 nm 99.2%.

S2.3 Synthesis of Bis(1,10-phenanthroline)(5-pyrenyl-1,10-phenanthroline)-ruthenium(II) chloride, $[Ru(phen)_2(phenPy)]Cl_2$ (RuphenPy)

RuphenPy was prepared from dichlorobis(1,10-phenanthroline)-ruthenium(II) (154 mg, 0.27 mmol) and **Py** (113 mg, 0.30 mmol) following the above-mentioned synthesis of **RubpyPy**. The PF_6 salt was obtained (154 mg, 52%) as raw product, of which 90 mg were converted to the chloride salt by ion exchange with *Amberlite IRA-410* (acetone). After removing the solvents under reduced pressure, the chloride salt of **RuphenPy** was purified by column chromatography (acetone/H_2O/sat. aqueous NaCl 40:20:1). The solvents were removed under reduced pressure and the product was then redissolved in acetone to separate it from excess chloride yielding **RuphenPy** (25 mg, 11%) as a red solid after solvent removal.

$\mathbf{R_f}$ = 0.48 (acetone/H_2O/sat. aqueous NaCl 40:20:1).

ESI-HRMS: Calcd. for $C_{52}H_{32}ClN_6Ru^+$ ([M-Cl]$^+$): m/z 877.1415, found: m/z 877.1418.

Calcd. for $C_{52}H_{32}N_6Ru^{2+}$ ([M-2Cl]$^{2+}$): m/z 421.0860, found: m/z 421.0871.

^{1}H NMR (400 MHz, CD_3CN): δ [ppm] = 8.76 – 8.60 (m, 5H), 8.51 – 8.18 (m, 12H), 8.17 – 8.04 (m, 7H), 8.02 – 7.87 (m, 2H), 7.85 – 7.78 (m, 1H), 7.77 – 7.61 (m, 4H), 7.43 – 7.36 (m, 1H).

HPLC (gradient with water 100% to acetonitrile 100%): purity at 254 nm 99.0%; purity at 450 nm 98.6%.

S3 Additional spectroscopic data and control experiments (steady-state)

S3.1 Concentration-dependence of UV-Vis spectra

To exclude solubility issues, the formation of aggregates and other concentration-dependent interferences during spectroscopic measurements, a Lambert-Beer plot was recorded for **RuphenPy** at the detection wavelength 450 nm (Fig. S1).

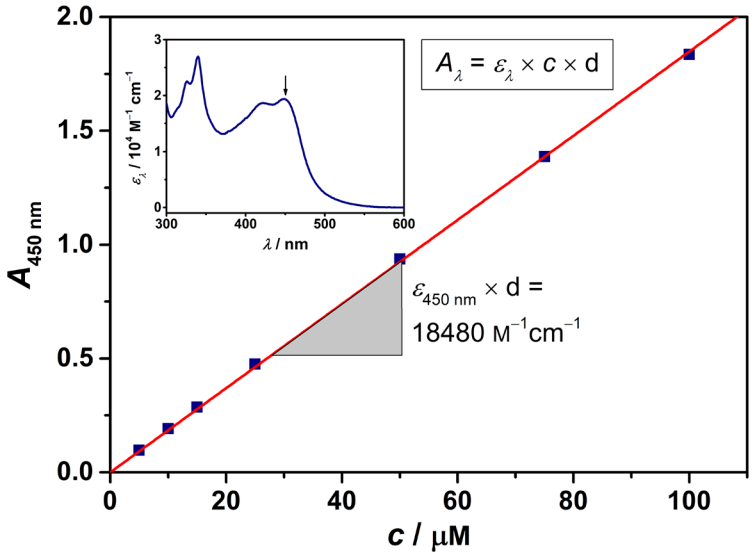

Fig. S1: Lambert-Beer plot of RuphenPy in H_2O at 450 nm recorded using cuvettes with 1 cm pathlength. The inset displays the calibrated UV-Vis spectrum of RuphenPy in water.

As shown in Fig. S1, the absorbance is linear with increasing sensitizer concentration and the slope directly corresponds to the molar absorption coefficient given that the cell thickness was 1 cm.

S3.2 Evidence for FRET upon pyrene excitation

To find evidence for the Förster resonance energy transfer (FRET) mechanism within the dyads, emission spectra of an aqueous 15 µM **RuphenPy** solution were measured at different excitation wavelengths (Fig. S2). As shown in Fig. 1 in the main paper, the absorption at 340 nm can predominantly be assigned to the **Py** ligand, while the absorption at 450 nm is metal centered.

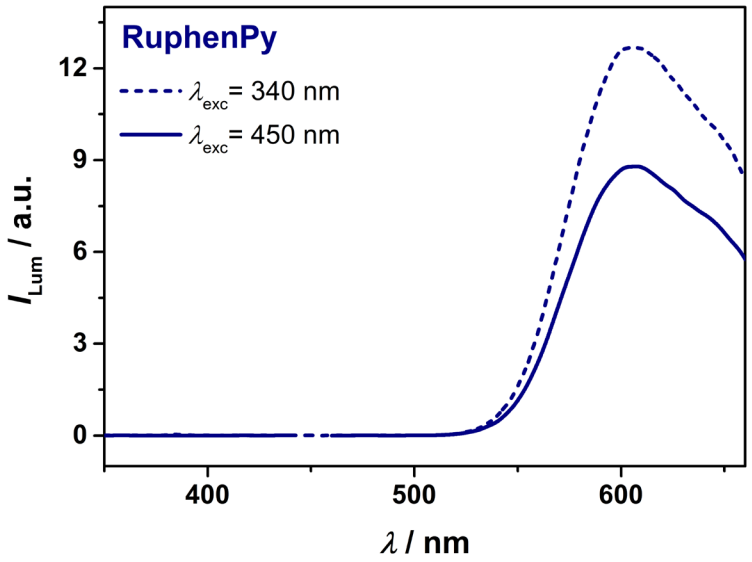

Fig. S2: Emission spectra of the same Ar-saturated aqueous RuphenPy solution (15 µM) measured at two different excitation wavelengths with an identical slit width of 5 nm (both for excitation and emission). For selective excitation of both chromophores in the dyad, 340 nm (dashed line, pyrene) and 450 nm (solid line, Ru complex) were used. Pyrene-based emission cannot be observed upon 340 nm excitation, providing indirect evidence for FRET.

Intense MLCT emission is clearly observable for both excitation settings. However, no fluorescence of the pyrene moiety (λ_{em}(**Py**) = 450 nm, Fig. 1 in the main paper) was observed at either excitation wavelength, indicating an effective FRET mechanism from the ^{1}pyrene* to the Ru complex upon 340 nm excitation.

S4 Laser flash photolysis and time-resolved spectroscopy

S4.1 Nanosecond LFP

Comparative spectroscopic data for RubpyPy and RuphenPy

A comparison of the emission spectra recorded with our laser setup for all four sensitizers is shown in Fig. S3. The emission maxima shift from **Rubpy** (center of the emission maximum at 610 nm) to shorter wavelengths (**RubpyPy**, 603 nm) and from **Ruphen** (590 nm) to longer wavelengths (**RuphenPy**, 597 nm) due to the change in the electronic structure of the ligand(s). The results of these measurements are in line with those obtained using a steady-state emission instrument (Fig. 1, main paper).

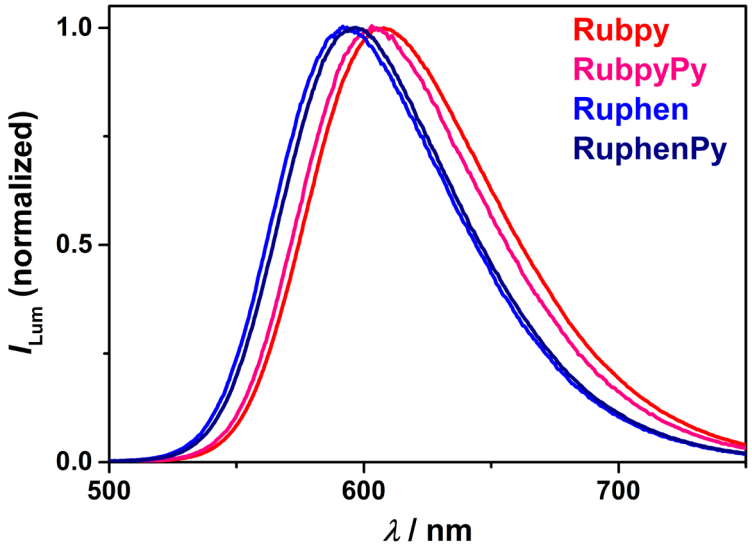

Fig. S3: Normalized spectral emission of the sensitizers Rubpy, Ruphen, RubpyPy and RuphenPy (30 µM each) in Ar-saturated aqueous solution upon excitation with 532 nm laser pulses (~50 mJ) recorded with integration times of the iCCD camera long enough for monitoring the complete excited state decay.

Fig. S4 turns to kinetic absorption traces of the dyads detected at wavelengths being characteristic for pyrene and its triplet state, namely 340 nm, 412 nm, and 512 nm. Measurements at these three wavelengths were considered for the determinations of the excited state lifetimes (Fig. 4, main paper). As described in the main paper, all emission- and absorption-based lifetimes are identical for each sensitizer, taking the experimental error (± 5%) into account.

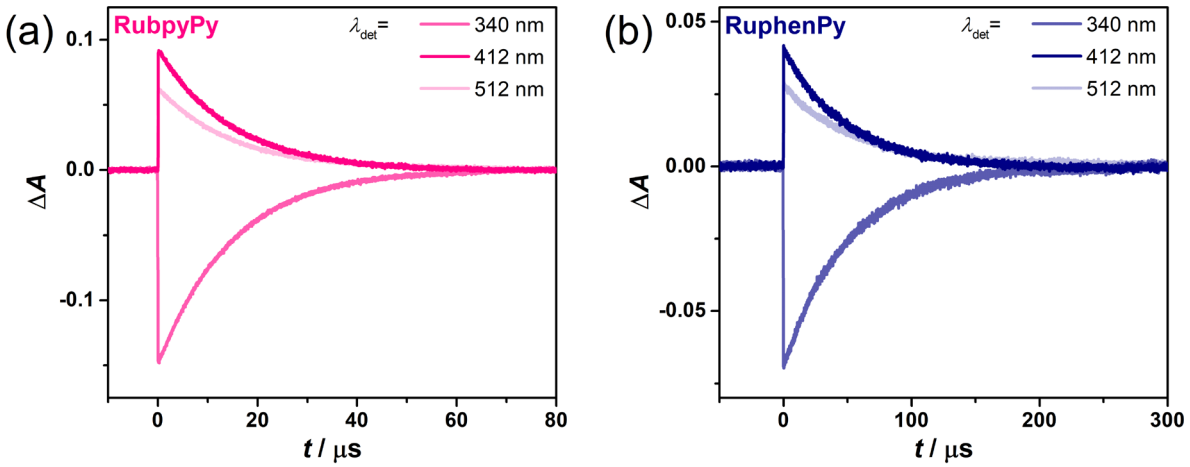

Fig. S4: Kinetic absorption traces of Ar-saturated aqueous solutions of RubpyPy (30 µM, a) and RuphenPy (30 µM, b) upon excitation with 532 nm laser pulses (35 mJ). The averaged excited state lifetimes are 14.5 µs (RubpyPy) and 52.6 µs (RuphenPy).

Temperature dependence of the excited state lifetime

The thermally activated population of the relatively short-lived ^{3}MLCT states in our dyads with long-lived pyrene-like lowest triplet states should be slowed down at lower temperatures, resulting in a pronounced temperature dependence. This aspect was investigated with our dyad **RuphenPy**, and indeed, lifetimes up to 113 µs are measured (5 °C), which decrease to 4 µs at 70 °C (Fig. S5). These results are in perfect agreement with the triplet reservoir effect. To reduce the probability of self-quenching, a particularly low **RuphenPy** concentration was chosen for these experiments.

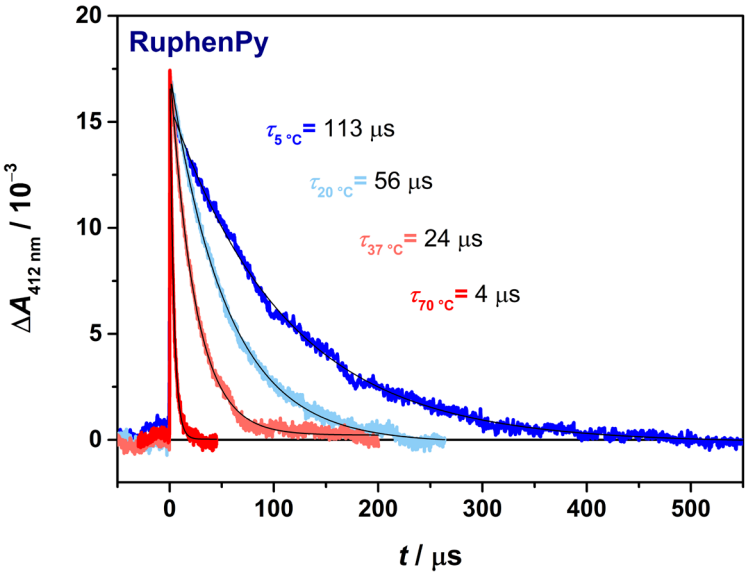

Fig. S5: Kinetic absorption traces and resulting lifetimes of Ar-saturated aqueous solutions of RuphenPy (15 µM) at four different temperatures (5 °C, 20 °C, 37 °C and 70 °C) upon excitation with 532 nm laser pulses (15 mJ) of *ca*. 10 ns duration.

pH dependence of the excited state lifetime

The excited state properties of **RuphenPy** were investigated at pH 2, 7 and 12 to illustrate that the sensitizer is highly photoactive regardless of the pH value of the aqueous solution. In pure water (without additives, pH ~7) an excited state lifetime slightly below 60 µs is achieved under the conditions of Fig. S6. This value is somewhat lower in $H_2SO_{4(aq)}$ and in $NaOH_{(aq)}$. The higher ionic strengths of these solutions facilitating self-quenching (owing to the kinetic salt effect) might provide an explanation for these minor lifetime decreases.

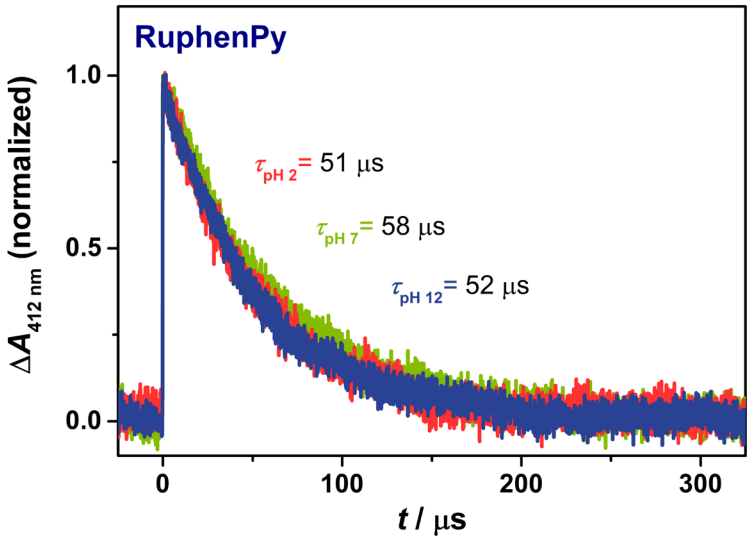

Fig. S6: Kinetic absorption traces and resulting lifetimes of Ar-saturated aqueous solutions of RuphenPy (15 µM) in H_2O (pH ~7), 5 mM $H_2SO_{4(aq)}$ (pH ~2) and 10 mM $NaOH_{(aq)}$ (pH ~12) upon excitation with 532 nm laser pulses (15 mJ) of *ca*. 10 ns duration.

MAMA triplet formation and decay

The data sets presented in Fig. S7 show transient absorption measurements monitoring the protonated 9-(methylaminomethyl)anthracene (MAMA) triplet after excitation of Ar-saturated solutions containing MAMA and one of the four sensitizers. The solutions were adjusted to pH 2 with hydrochloric acid to ensure solubility of MAMA. Kinetic absorption signals were measured at 425 nm and the corresponding triplet spectrum (which agrees with that in the literature)[1] was recorded 15 µs after laser excitation of the **RuphenPy**-containing solution such that the excited state of **RuphenPy** has already decayed.

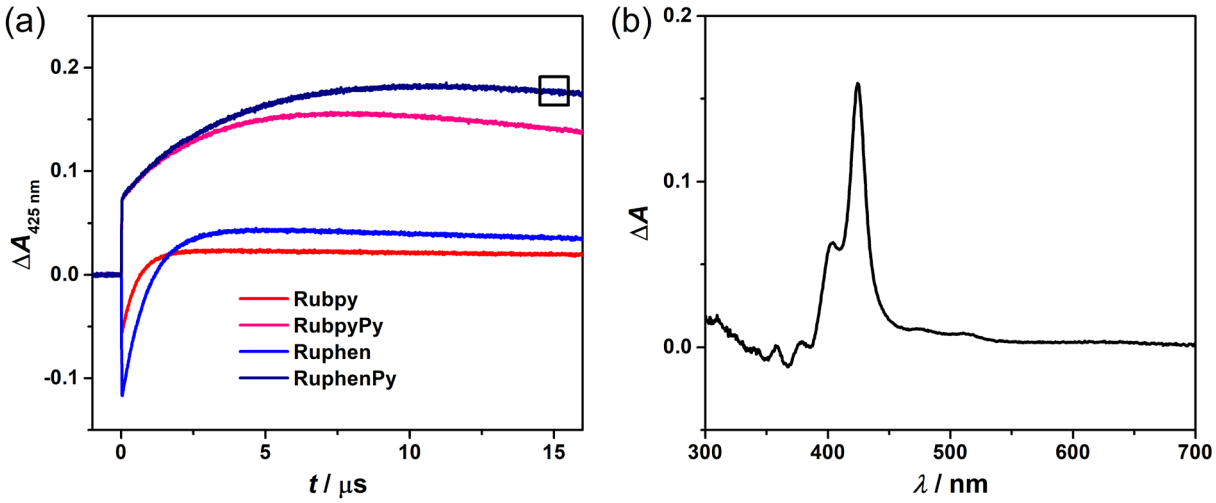

Fig. S7: (a) Kinetic absorption traces at 425 nm of Ar-saturated aqueous solutions at pH 2.0 containing the sensitizer Rubpy, RubpyPy, Ruphen or RuphenPy (30 µM each) and MAMA (0.1 mM). (b) Triplet spectrum of MAMA (0.1 mM) in deoxygenated water at pH 2.0 in the presence of RuphenPy (30 µM) 15 µs after laser excitation (black square in (a)). For all experiments, green (532 nm) laser pulses with an intensity of 100 mJ were used and all solutions were adjusted to an absorbance of 0.021 at the excitation wavelength. The signals in (a) right after the laser pulse are due to ^{3}MLCT (negative signals at 425 nm) or ^{3}pyrene (positive signals at 425 nm) formation.

Bimolecular energy transfer with Rubpy and Ruphen

The triplet-triplet energy transfer (EnT) between the Ru complexes and the pyrene-containing ligand can also be observed bimolecularly. In this case, absorption bands arise at 415 nm and 515 nm on a timescale of a few hundreds of nanoseconds when a solution of **Rubpy** or **Ruphen** and the **Py** ligand in acetonitrile is irradiated with laser pulses at 532 nm. These absorption bands are very characteristic and can be assigned to the pyrene-localized triplet.[5–7] Kinetic measurements revealed a simultaneous increase of the 515 nm band with decreasing emission of the sensitizer at 620 nm (**Rubpy**) or 600 nm (**Ruphen**) (Fig. S8a and c). This behavior indicates the intermolecular energy transfer between the two chromophores and Stern-Volmer analyses resulted in quenching constants of 1.5×10^9 M^{-1} s^{-1} for **Rubpy** and 3.9×10^9 M^{-1} s^{-1} for **Ruphen** (Fig. S8b and d). The measured natural lifetimes of **Rubpy** and **Ruphen** in acetonitrile were 890 ns and 470 ns, respectively, which are consistent with literature data.[7]

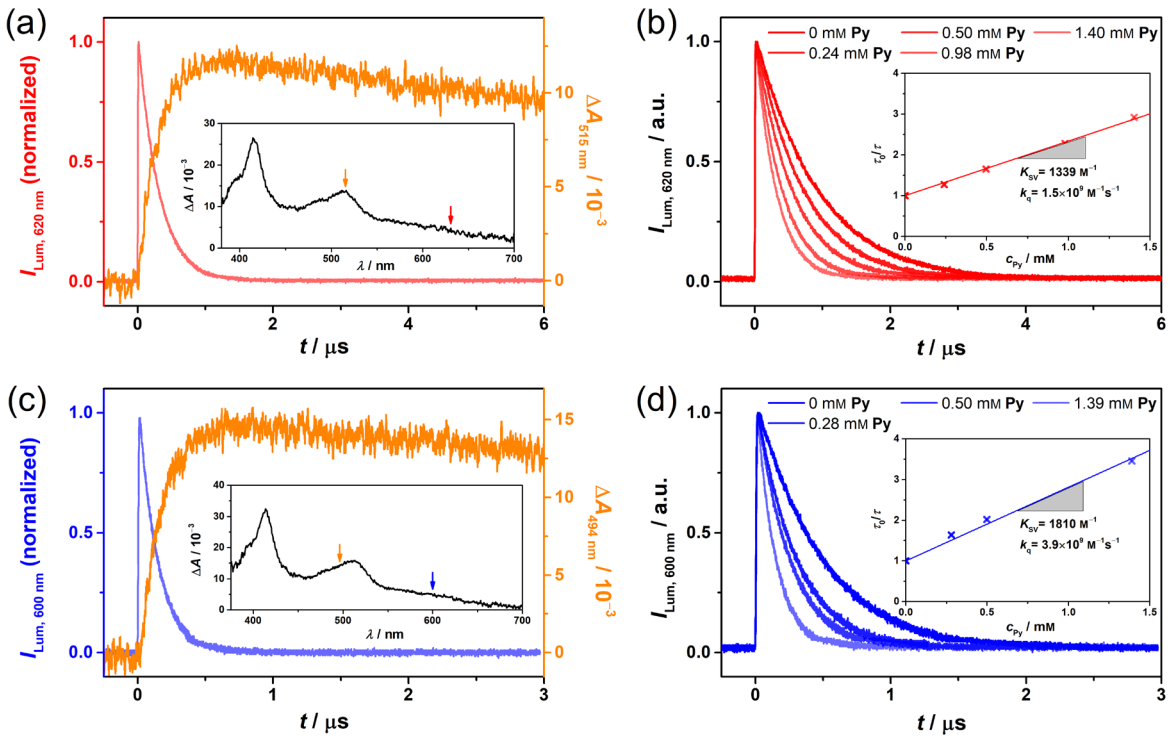

Fig. S8: Intermolecular energy transfer between 30 µM $[Ru(bpy)_3](PF_6)_2$ (a, b) or 30 µM $[Ru(phen)_3](PF_6)_2$ (c, d) and Py in Ar-saturated acetonitrile solutions after excitation with 532 nm laser pulses (30 mJ). (a) Formation of the pyrene-localized triplet (absorption at 515 nm, orange) and simultaneous decay of Rubpy emission at 620 nm (red) (with 1.40 mM of Py); inset, transient absorption spectra of the same solution 2 µs after laser excitation. (b) Stern-Volmer analysis of the Rubpy lifetime quenching with varying Py concentrations. (c) Emission decay of Ruphen at 600 nm (blue) and formation of the pyrene-localized triplet at the isosbestic point between Ruphen and ^{3}Ruphen (494 nm) in a 1.39 mM Py solution; inset, transient absorption spectra of the same solution 1 µs after laser excitation. (d) Stern-Volmer analysis of the Ruphen lifetime quenching with varying Py concentrations.

S4.2 Ultrafast transient absorption spectroscopy (fs-TAS)

fs-TAS experiments were performed employing the pump-supercontinuum-probe technique.[8] 800 nm pulses with 35 fs width were generated at 1 kHz repetition rate employing a regenerative Ti:sapphire laser amplifier (Spitfire 9886A, *Spectra-Physics*), which was seeded by an 80 MHz Ti:sapphire oscillator (Tsunami 360, *Spectra-Physics*). The laser output was frequency doubled in a 0.5 mm β-barium borate crystal and the resulting 400 nm beam was split into the pump and the probe beam path.

For the excitation, the pump was chopped at a frequency of 500 Hz and attenuated to a pulse energy of 500 nJ/pulse using a λ/2-waveplate and a linear polarizer.

A broadband UV-VIS-supercontinuum covering the spectral range between 320 nm and 600 nm was generated by focusing the attenuated (15 nJ/pulse) second part of the 400 nm beam into water, which was circulated in a flow-through cuvette (10 mm optical path length). The resulting supercontinuum was split into a probe and a reference beam path. For acquiring the TAS signal, the probe and the reference were imaged separately onto the entrance slits of two grating spectrographs and projected on 512-element Si photodiode array detectors.

The sample solutions (0.1 mM in deaerated water) were measured in a 1 mm quartz cuvette. The pump and the probe pulses were focused into the cuvette where they were overlapped. At the sample position, the beam diameter of the pump and the probe was 260 µm and 160 µm, respectively. The time delay between pump and probe was controlled with an optical delay line (*OWIS*, 250 mm). The instrument response function had a width of *ca.* 120 fs.

Global analysis of the TA data was performed employing the well-established software *Glotaran*.[9]

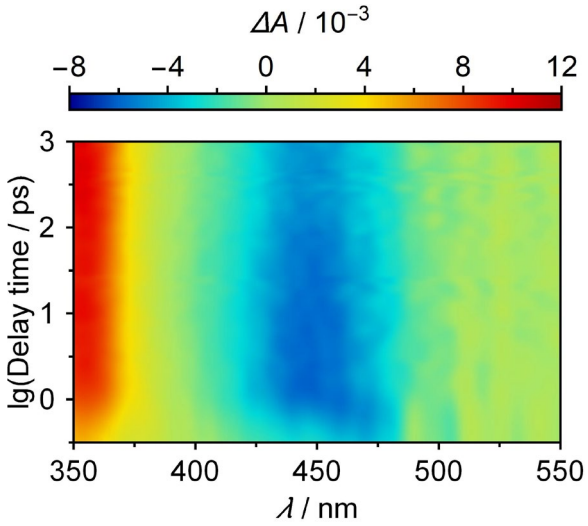

Fig. S9: Contour map of the fs-TA spectra of an Ar-saturated aqueous solution of Rubpy (0.1 mM) after excitation with 400 nm laser pulses of 35 fs duration (500 nJ/pulse).

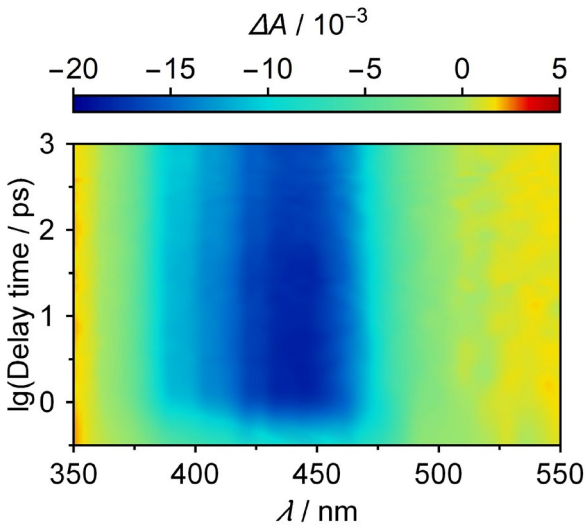

Fig. S10: Contour map of the fs-TA spectra of an Ar-saturated aqueous solution of Ruphen (0.1 mM) after excitation with 400 nm laser pulses of 35 fs duration (500 nJ/pulse).

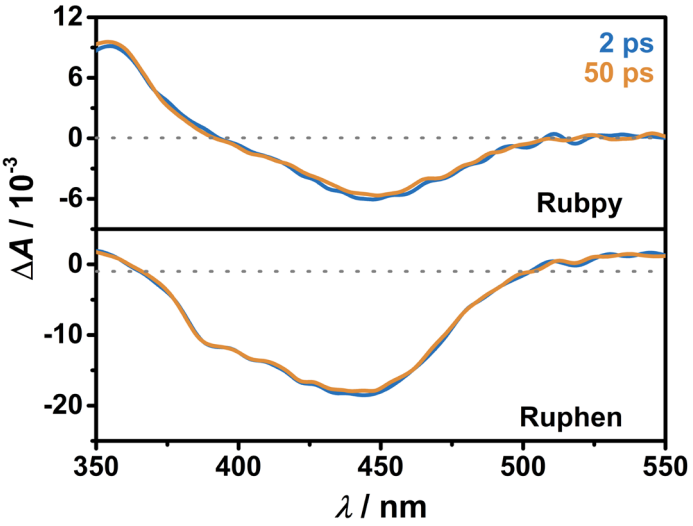

Fig. S11: Transient absorption spectra of aqueous solutions (0.1 mM) containing Rubpy (top) or Ruphen (bottom) upon excitation with laser pulses of 35 fs duration at 400 nm (500 nJ/pulse).

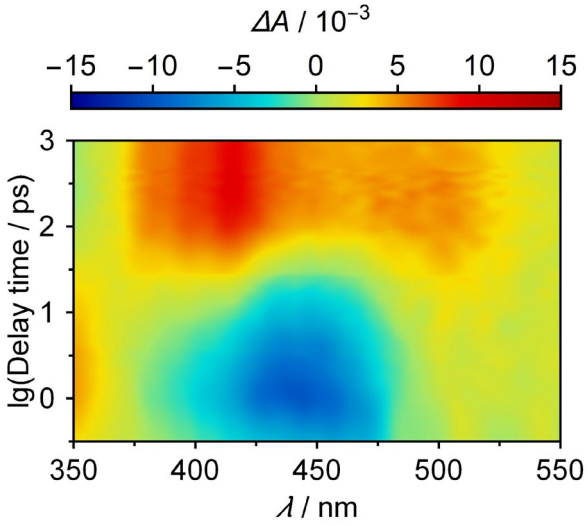

Fig. S12: Contour map of the fs-TA spectra of an Ar-saturated aqueous solution of RubpyPy (0.1 mM) after excitation with 400 nm laser pulses of 35 fs duration (500 nJ/pulse).

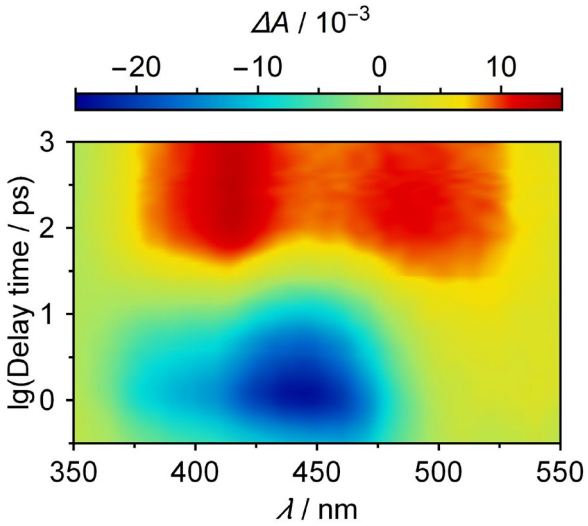

Fig. S13: Contour map of the fs-TA spectra of an Ar-saturated aqueous solution of RuphenPy (0.1 mM) after excitation with 400 nm laser pulses of 35 fs duration (500 nJ/pulse).

Tab. S1: Fitting parameters of the best-fit functions ($a\ e^{-t/\tau_1} + b\ e^{-t/\tau_2}$) for the corresponding transient absorption traces at 420 nm and 490 nm / 500 nm in Fig. 2b (main paper).

	λ / nm	a_{norm}	τ_1 / ps	b_{norm}	τ_2 / ps
RubpyPy	420	0.28	7	0.72	46
	490	0.17	7	0.83	46
RuphenPy	420	0.23	4	0.77	25
	500	0.18	4	0.82	25

S4.3 Kinetic considerations

Dissolved oxygen and several other potential energy acceptors have a low solubility in water, typically resulting in inefficient energy transfer processes and low reaction quantum yields. The kinetic simulation displayed in Fig. S14 illustrates the need for long triplet lifetimes of the sensitizers for reactions that cannot be carried out at high acceptor/substrate concentrations. Even with second-order rate constants at the diffusion limit, the quenching efficiencies are below 50% when sensitizers such as **Rubpy** (triplet lifetime, 600 ns) are employed. In contrast, the energy is transferred with efficiencies close to unity when long-lived triplets are used as sensitizers (e.g. a dyad with τ_0 = 60 µs). The usage of such long-lived triplet energy donors would also result in quenching efficiencies beyond 85% for energy transfer reactions with much slower bimolecular rate constants, as displayed in Fig. S14.

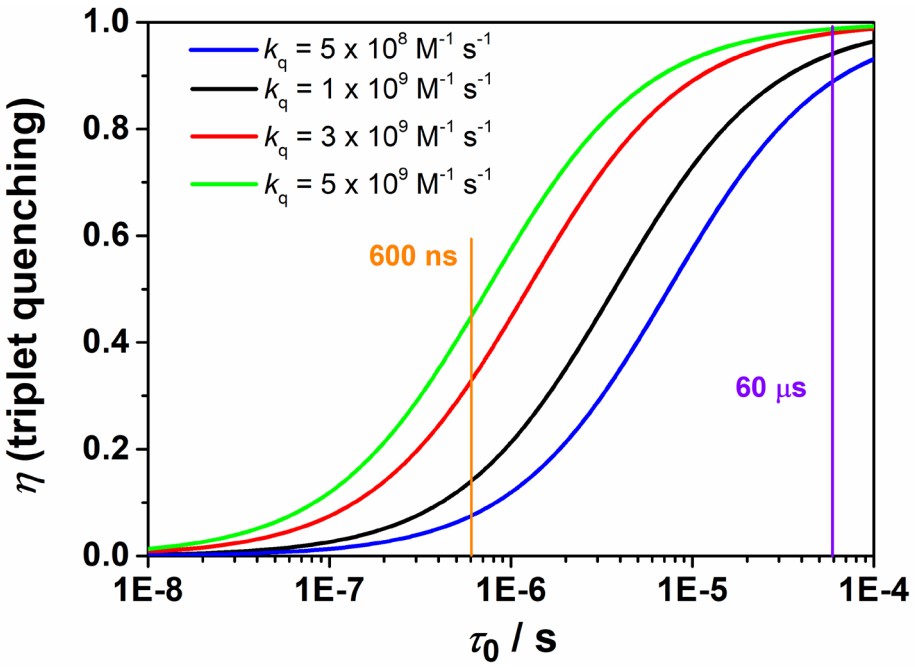

Fig. S14: Predicted quenching efficiencies at a standardized quencher concentration (0.27 mM, corresponding to solubility of dissolved oxygen in air-saturated water) as a function of the natural (unquenched) photosensitizer lifetime at four different quenching rate constants. This kinetic simulation was performed using the well-known kinetic equations for bimolecular excited-state quenching.[10]

S5 Singlet-oxygen formation and energy-transfer photocatalysis

S5.1 Absorption spectra of the Imd/RNO method and control experiments

Fig. S15 displays the absorption spectra of all four sensitizers (**Rubpy**, **Ruphen**, **RubpyPy**, **RuphenPy**) that were used to quantify their $^1O_2$ formation properties through the imidazole plus *p*-nitroso-dimethylaniline (Imd/RNO) method.[11] These data sets served as raw date for the analysis included in the main paper (Fig. 5). The irradiation was carried out in air-saturated solution with the PR160L 525 nm LED operating at 25% output power.

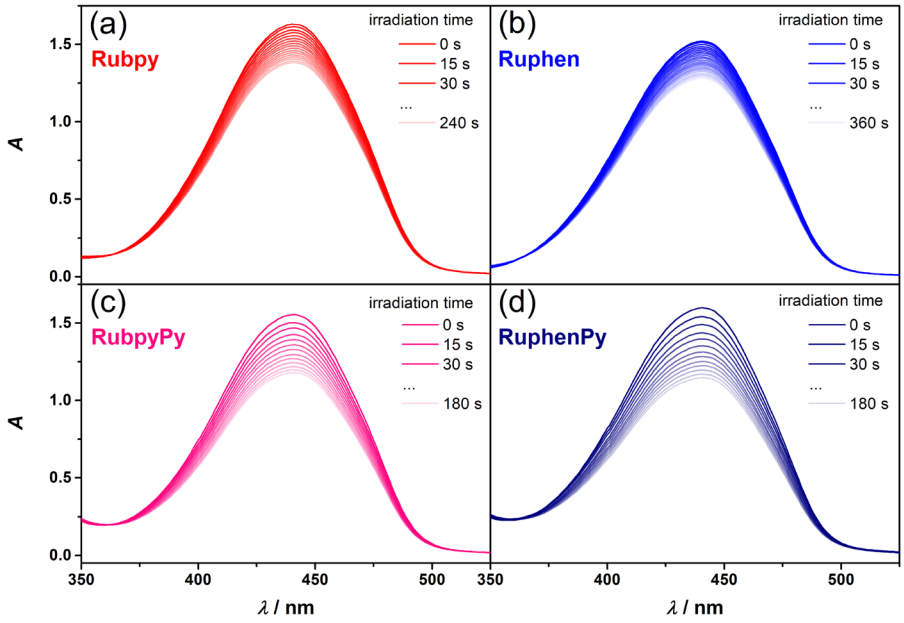

Fig. S15: Absorption spectra of air-saturated aqueous solutions of RNO (40 µM), imidazole (8 mM) and the respective sensitizer (10 µM) in phosphate buffer (10 mM) before and during (15 s intervals) irradiation with a 525 nm LED at 25% power intensity until the absorption band of RNO at 440 nm has decreased to about 85%.

To avoid side and secondary reactions of degradation products, only the initial range was considered for the evaluation (decrease of RNO absorption band to about 85% compared to the starting value). Further control experiments were performed, showing that bleaching of RNO proceeds exclusively via the proposed pathway (Fig. 5b, main paper). Irradiation experiments in the absence of Imd and/or the sensitizer resulted in essentially no bleaching of the RNO absorption band (Fig. S16a-c) despite extended irradiation times at higher LED intensities.

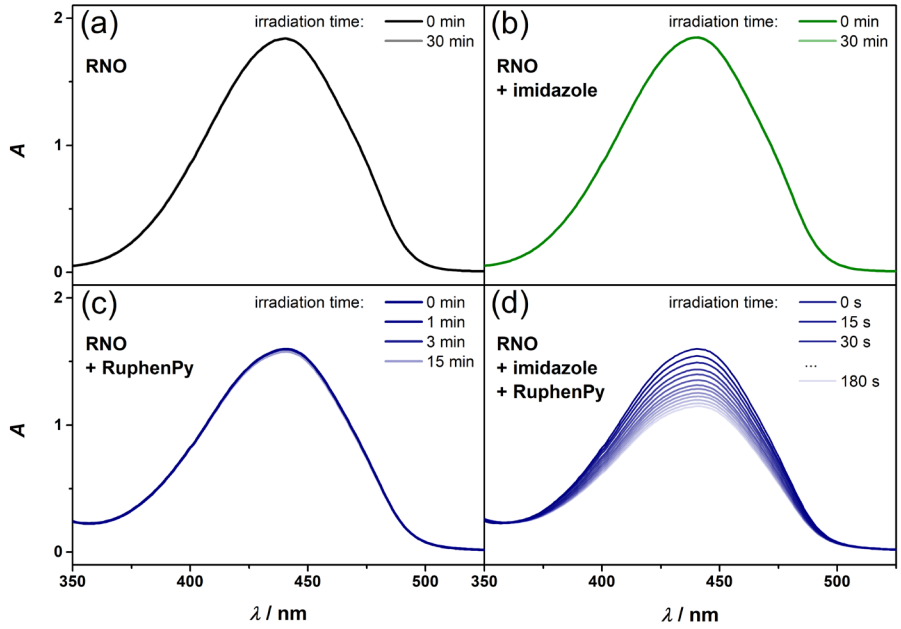

Fig. S16: Absorption spectra of phosphate buffered (10 mM) air-saturated aqueous solutions of (a) 50 µM RNO, (b) 50 µM RNO and 8 mM imidazole, (c) 40 µM RNO and 10 µM RuphenPy, and (d) 40 µM RNO, 8 mM imidazole and 10 µM RuphenPy before and after irradiation with a 525 nm LED. The output power was set to 100% for (a)–(c) and 25% for (d).

S5.2 Details and control experiments for the $^1O_2$-mediated oxidation of 5-HMF

To investigate the photosensitized $^1O_2$ production by **RuphenPy** on laboratory scale, the oxidation of 5-(hydroxymethyl)furfural (5-HMF) was employed, in which an α,β-unsaturated lactone and a C_1-building block can be obtained from a bioavailable starting material[12,13] in neat water. Therefore, an air-saturated aqueous solution containing **RuphenPy** (0.2 mol%) and 5-HMF (30 mM) was irradiated with the 525 nm LED at room temperature and a power setting of 100%. During the entire irradiation time, air was passed through the solution using a septum, two cannulas and slight vacuum (see Fig. S20 for the setup). After nine hours of irradiation, 5-HMF was oxidized with a yield of 80% to the respective lactone in the presence of **RuphenPy**, while the solution without sensitizer did not show any conversion (Fig. S17). The reaction was monitored by ^{1}H NMR spectroscopy. For quantitative analysis of both conversion and product yield, sodium acetate was added as reference (singlet at δ = 1.92 ppm)[14]. Its chemical shift slightly changes during irradiation due to the decreasing pH (formation of formic acid) in the reaction flask upon irradiation.

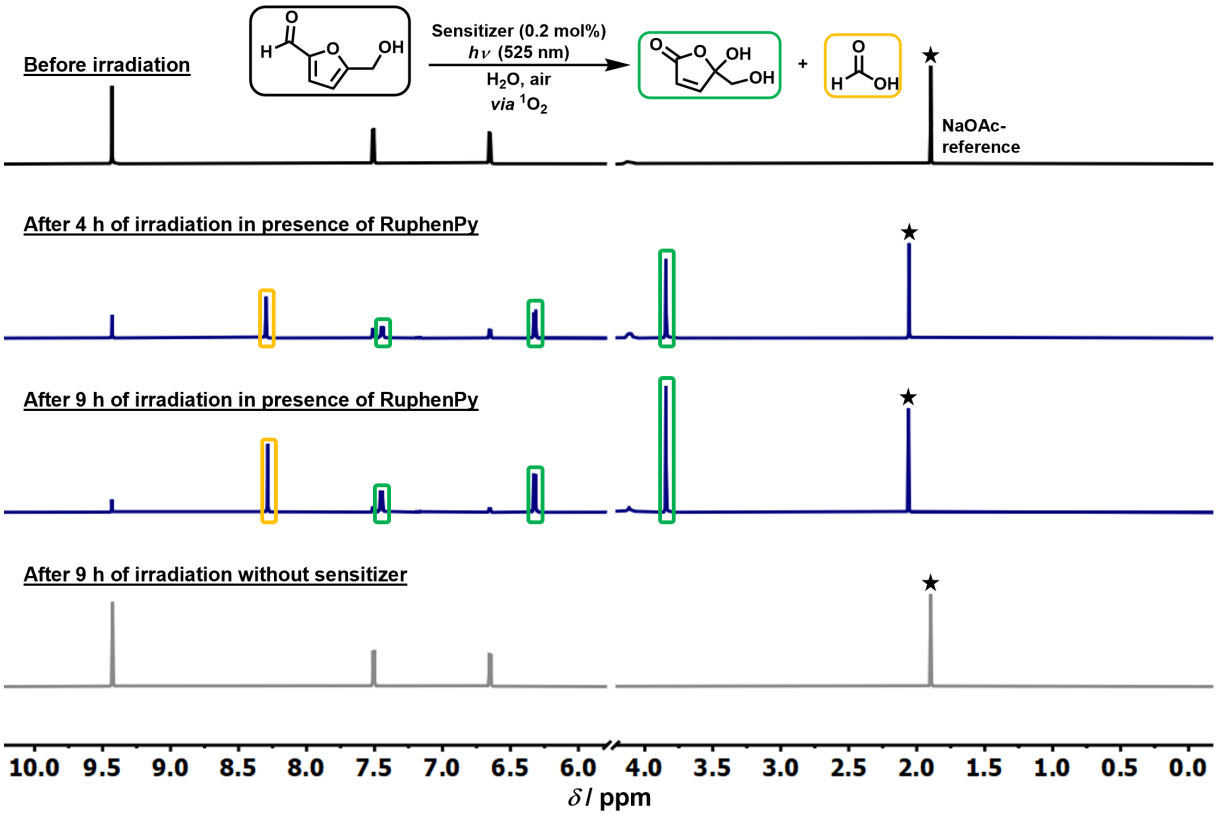

Fig. S17: ^{1}H NMR spectra of the $^{1}O_2$ oxidation of 5-HMF. The solutions contained 30 mM 5-HMF and 0.2 mol% sensitizer in neat water (i.e. without pH-active additives) as solvent and were irradiated with a PR160L 525 nm LED from Kessil Science at a power setting of 100%. The emission spectrum of the LED and a photograph of the irradiation setup and can be found in the appendix (Fig. S19 and Fig. S20). The signal of the reference sodium acetate was marked with an asterisk.

In contrast to the neutral-to-acidic pH conditions described above, oxidation in alkaline solution (1.5 eq. NaOH, pH ~12.5) proceeds with simultaneous ring opening of the lactone (scheme in Fig. S18). The resulting compound appears to exhibit increased reactivity leading to oligomerization[15] at basic pH and room temperature (light gray boxes in Fig. S18). To prevent this, the reaction mixture was cooled with an ice bath during irradiation and well-defined doublets at 6.46 ppm and 6.17 ppm as well as a singlet at 4.42 ppm emerge in the NMR spectra, indicating the formation of one main product (in addition to the co-product formic acid). We assigned these signals to (*Z*)-5-hydroxy-4-keto-2-pentenoic acid. Due to the lack of literature spectra of this reactive compound, the signals were compared to those of the well-characterized and structurally related 4-oxohex-2-enoic acid.[16,17] Owing to the coupling constant of 12.2 Hz of the doublets (see roofing in the inset of row 3 of Fig. S18), we conclude that the *cis* isomer of 5-hydroxy-4-keto-2-pentenoic acid is formed (coupling constants for 4-oxohex-2-enoic acid: *cis*, 12.2 Hz; *trans*, 16.0 Hz). The 5-HMF conversion of the irradiation experiment under basic conditions at room temperature was 89% and decreased slightly to 81% under ice cooling with significantly increased selectivity towards the open chain product. However, it was found that in addition to pH-dependent product formation, the NMR signals of the entire system are

sensitive to pH. Thus, especially the doublet at 6.17 ppm shows a pronounced broadening at longer irradiation times and the associated increase in formic acid (see insets in row 3 and 4 of Fig. S18). As in previous irradiation experiments, the yield calculation of (*Z*)-5-hydroxy-4-keto-2-pentenoic acid was performed by integrating and averaging the signals of the double bond protons relative to the internal standard sodium acetate. For the ice-cooled irradiation reaction, the yield was 62%. In contrast to the irradiation reaction in neutral-to-acidic solution (Fig. S17), the yield determination via the proton signal of the formate (δ = 8.42 ppm[14]) gave a higher value than for the C_5 building block. This can be explained by a subsequent reaction in which maleic acid is formed from (*Z*)-5-hydroxy-4-keto-2-pentenoic acid by oxidative cleavage, thereby generating a further equivalent of formic acid. This is consistent with the signal occurring at 6.01 ppm in the NMR (maleic acid[18]) and the decrease in pH, which can be followed by the chemical shift of the sodium acetate and the signal width of the double bond protons of the open chain product. For verification, an authentic sample of the C_4 compound maleic acid was also added to the reaction mixture (into the NMR tube after irradiation) as a reference and the signals are in perfect agreement. The NMR yield of maleic acid after nine hours of irradiation in ice-cooled basic solution is 11%. As a further indication of the tendency of (*Z*)-5-hydroxy-4-keto-2-pentenoic acid to polymerize, no protons of the double bond could be detected in the NMR spectrum after storing the reaction mixture containing the open chain product for one day at room temperature in the dark (row 5 of Fig. S18).

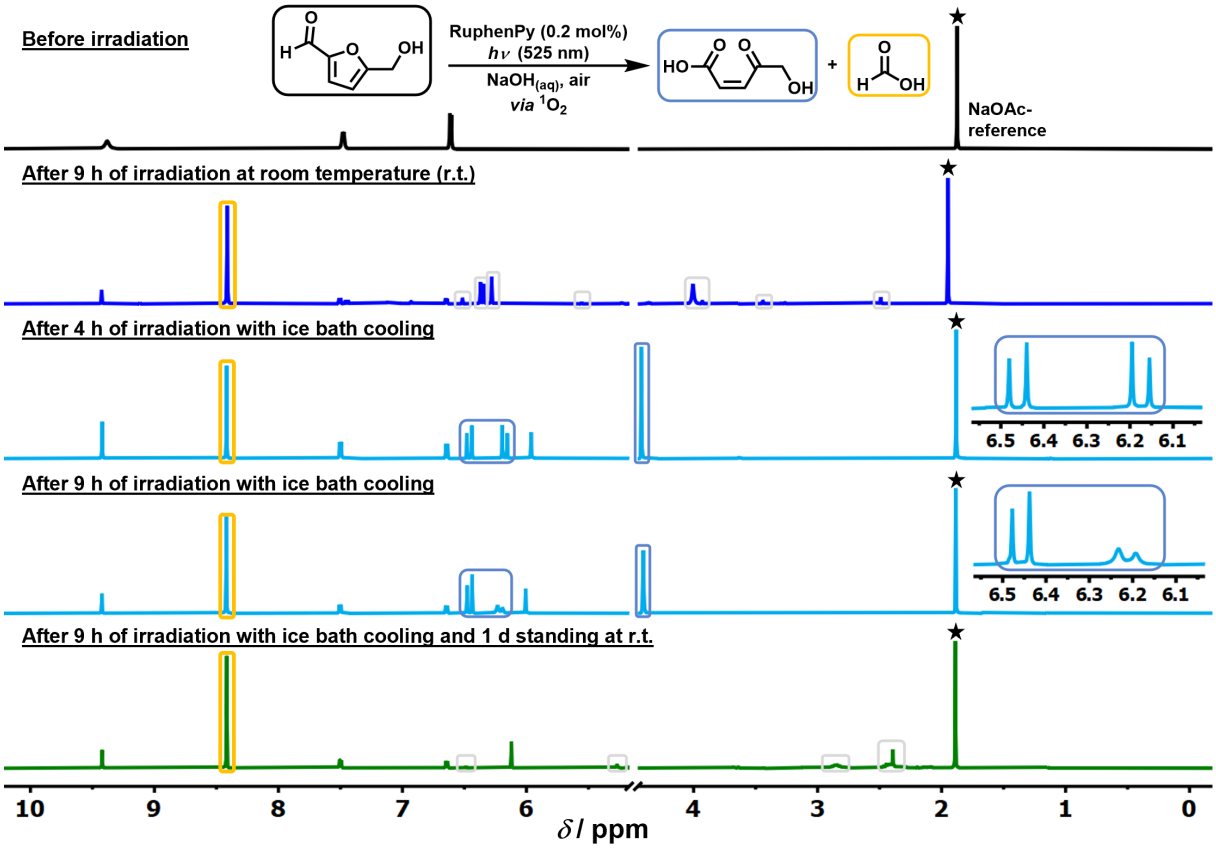

Fig. S18: ^{1}H NMR spectra of the $^1O_2$ oxidation of 5-HMF. The solutions contained 30 mM 5-HMF and 0.2 mol% sensitizer in aqueous NaOH (45 mM) as solvent and were irradiated with a PR160L 525 nm LED from Kessil Science at a power setting of 100%. Color-coded boxes indicate the NMR signals of the reactant and products, gray boxes are assigned to undesired side products and oligomers. Due to the broadening of the aldehyde signal under basic conditions, the aldehyde signal of the reactant appears smaller than in neutral solution (Fig. S17), but an integration over the signal matches the initial concentration. The signal of the reference sodium acetate was marked with an asterisk. See text for further explanations.

S6 Supplementary references

1 C. Kerzig and O. S. Wenger, *Chem. Sci.*, 2018, **9**, 6670–6678.

2 Kessil, Kessil Science PR160L, https://kessil.com/science/PR160L.php (accessed March 2022).

3 H. E. Gottlieb, V. Kotlyar and A. Nudelman, *J. Org. Chem.*, 1997, **62**, 7512–7515.

4 M. J. Frisch, G. W. Trucks, H. B. Schlegel, G. E. Scuseria, M. A. Robb, J. R. Cheeseman, G. Scalmani, V. Barone, B. Mennucci, G. A. Petersson, H. Nakatsuji, M. Caricato, X. Li, H. P. Hratchian, A. F. Izmaylov, J. Bloino, G. Zheng, J. L. Sonnenberg, M. Hada, M. Ehara, K. Toyota, R. Fukuda, J. Hasegawa, M. Ishida, T. Nakajima, Y. Honda, O. Kitao, H. Nakai, T. Vreven, J. A. Montgomery, J. E. Peralta, F. Ogliaro, M. Bearpark, J. J. Heyd, E. Brothers, K. N. Kudin, V. N. Staroverov, R. Kobayashi, J. Normand, K. Raghavachari, A. Rendell, J. C. Burant, S. S. Iyengar, J. Tomasi, M. Cossi, N. Rega, J. M. Millam, M. Klene, J. E. Knox, J. B. Cross, V. Bakken, C. Adamo, J. Jaramillo, R. Gomperts, R. E. Stratmann, O. Yazyev, A. J. Austin, R. Cammi, C. Pomelli, J. W. Ochterski, R. L. Martin, K. Morokuma, V. G. Zakrzewski, G. A. Voth, P. Salvador, J. J. Dannenbaerg, S. Dapprich, A. D. Daniels, Farkas, J. B. Foresman, J. V. Ortiz, J. Cioslowski and D. J. Fox, *Gaussian 09 Revision B.01*, 2010.

5 D. S. Tyson, K. B. Henbest, J. Bialecki and F. N. Castellano, *J. Phys. Chem. A*, 2001, **105**, 8154–8161.

6 C. Kerzig and M. Goez, *Chem. Sci.*, 2016, **7**, 3862–3868.

7 M. Montalti, A. Credi, L. Prodi and M. T. Gandolfi, *Handbook of Photochemistry*, CRC/Taylor & Francis, Boca Raton, 3rd ed., 2006.

8 A. L. Dobryakov, S. A. Kovalenko, A. Weigel, J. L. Pérez-Lustres, J. Lange, A. Müller and N. P. Ernsting, *Rev. Sci. Instrum.*, 2010, **81**, 113106.

9 I. H. M. van Stokkum, D. S. Larsen and R. van Grondelle, *Biochim. Biophys. Acta*, 2004, **1657**, 82–104.

10 F. Glaser, C. Kerzig and O. S. Wenger, *Angew. Chem. Int. Ed.*, 2020, **59**, 10266–10284.

11 I. Kraljić and S. E. Mohsni, *Photochem. Photobiol.*, 1978, **28**, 577–581.

12 K. I. Galkin and V. P. Ananikov, *ChemSusChem*, 2019, **12**, 2976–2982.

13 J. J. Bozell and G. R. Petersen, *Green Chem.*, 2010, **12**, 539–554.

14 A. M. King, H. A. Sparkes, R. L. Wingad and D. F. Wass, *Organometallics*, 2020, **39**, 3873–3878.

15 T. S. A. Heugebaert, C. V. Stevens and C. O. Kappe, *ChemSusChem*, 2015, **8**, 1648–1651.

16 C. Xu, X. Bai, J. Xu, J. Ren, Y. Xing, Z. Li, J. Wang, J. Shi, L. Yu and Y. Wang, *RSC Adv.*, 2017, **7**, 4763–4775.

17 S. Seltzer and K. D. Stevens, *J. Org. Chem.*, 1968, **33**, 2708–2711.

18 C. Kerzig and O. S. Wenger, *Chem. Sci.*, 2019, **10**, 11023–11029.

19 G. R. Fulmer, A. J. M. Miller, N. H. Sherden, H. E. Gottlieb, A. Nudelman, B. M. Stoltz, J. E. Bercaw and K. I. Goldberg, *Organometallics*, 2010, **29**, 2176–2179.

20 E. Kang, H. R. Park, J. Yoon, H.-Y. Yu, S.-K. Chang, B. Kim, K. Choi and S. Ahn, *Microchem. J.*, 2018, **138**, 395–400.

S7 Appendix

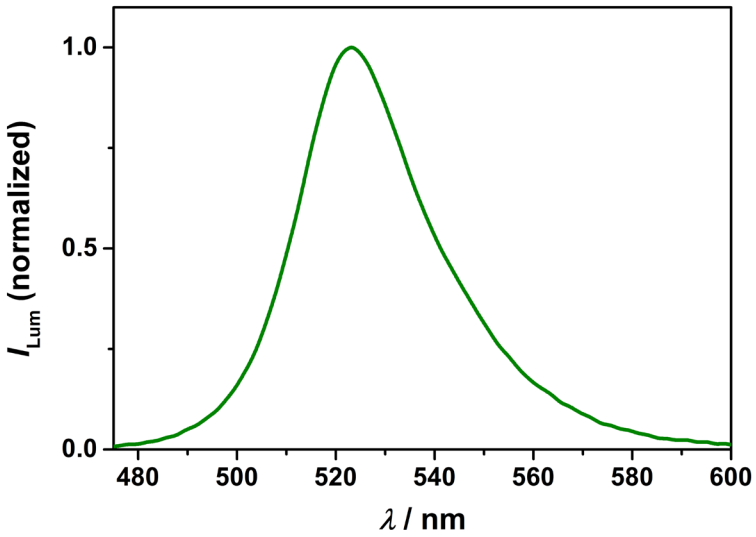

Fig. S19: Normalized emission spectrum of the PR160L 525 nm LED from Kessil Science. The emission spectrum was measured by irradiating a water-containing cuvette in the emission spectrometer (i.e., by measuring scattering light).

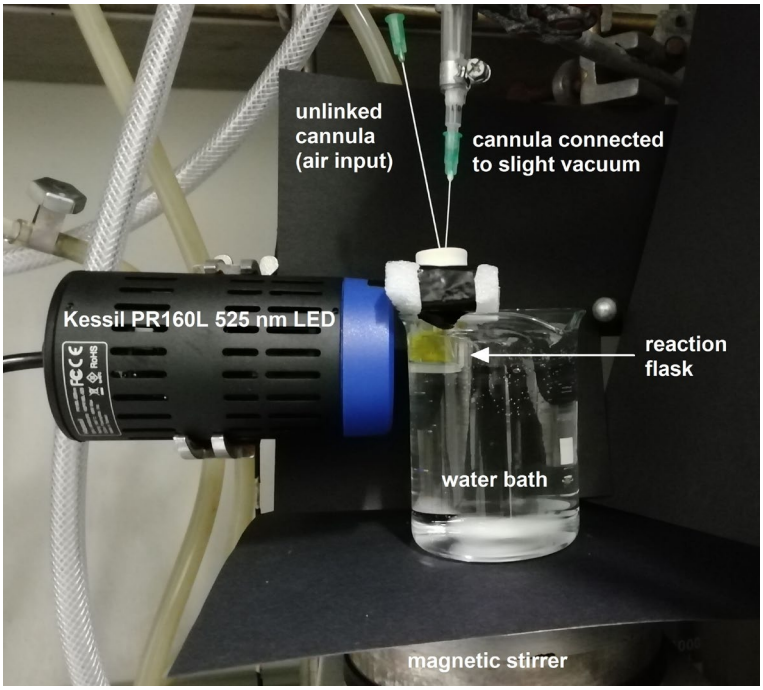

Fig. S20: Experimental irradiation setup for $^1O_2$ oxidation of 5-HMF in air-saturated solution with the respective sensitizer (Section S5.2).

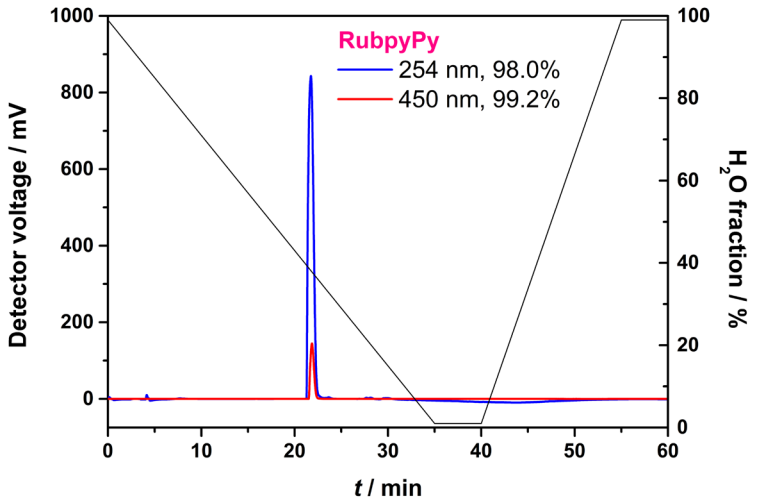

Fig. S21: HPLC chromatogram for purity determination of RubpyPy using a water-acetonitrile solvent gradient and UV-Vis analysis at 254 nm and 450 nm.

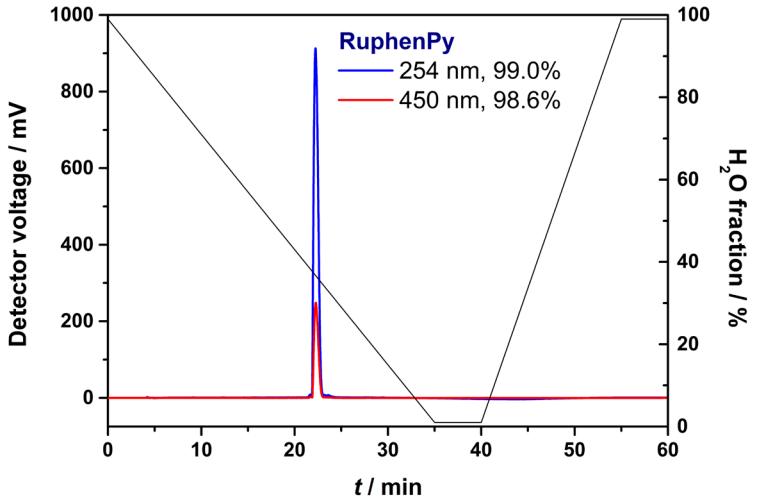

Fig. S22: HPLC chromatogram for purity determination of RuphenPy using a water-acetonitrile solvent gradient and UV-Vis analysis at 254 nm and 450 nm.

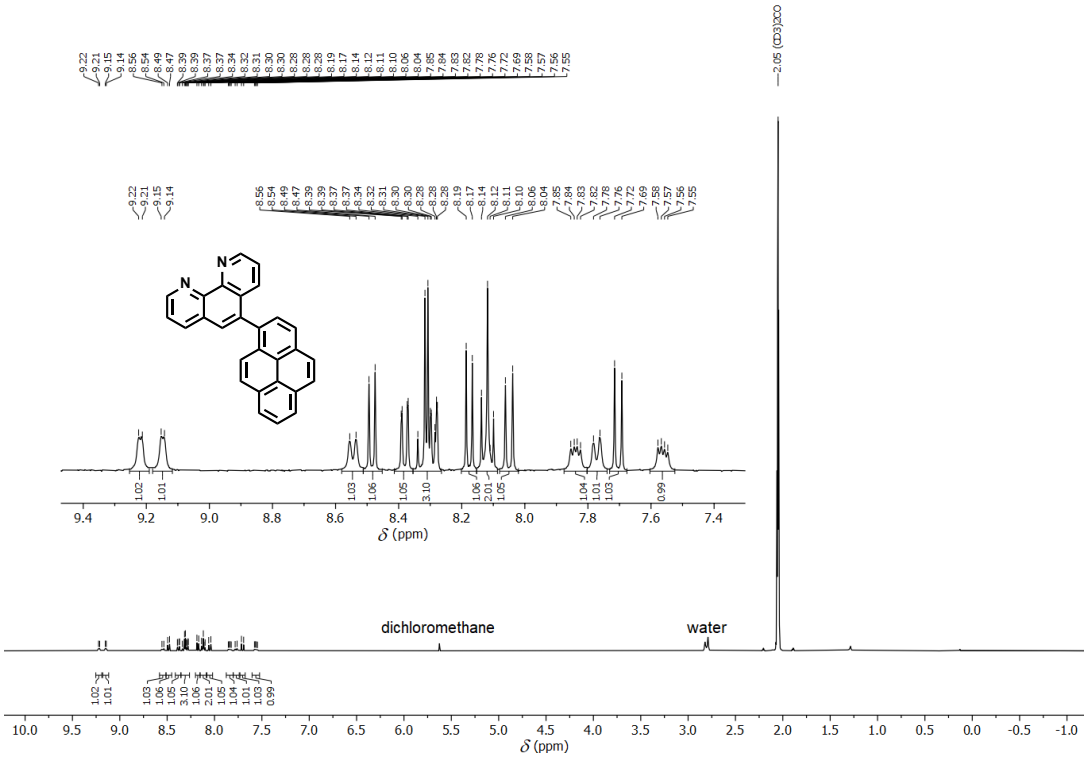

Fig. S23: ^{1}H NMR spectrum (400 MHz, acetone-d_6) of Py (main plot) and aromatic region on enlarged scale (inset). The relatively low signal intensity can be attributed to the limited solubility of Py in acetone. The weak signals in the aliphatic region can be assigned to the solvents used during purification.[3,19]

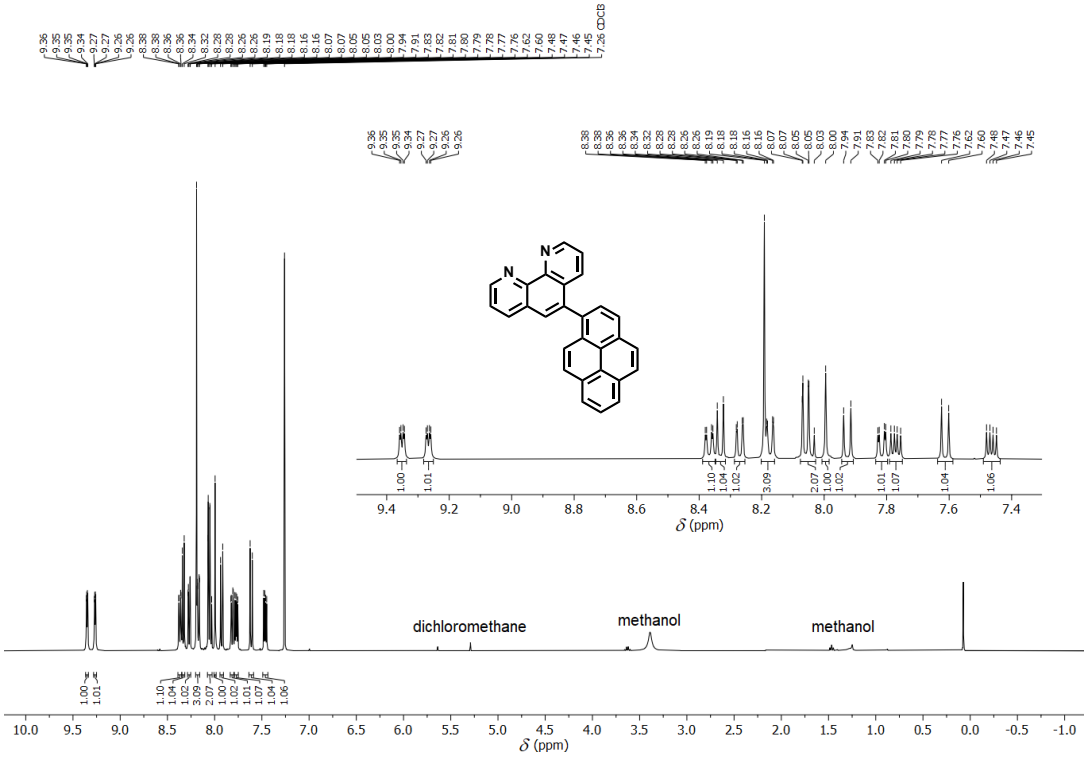

Fig. S24: ^{1}H NMR spectrum (400 MHz, $CDCl_3$) of Py (main plot) and aromatic region on enlarged scale (inset). The weak signals in the aliphatic region can be assigned to the solvents used during purification.[3,19,20]

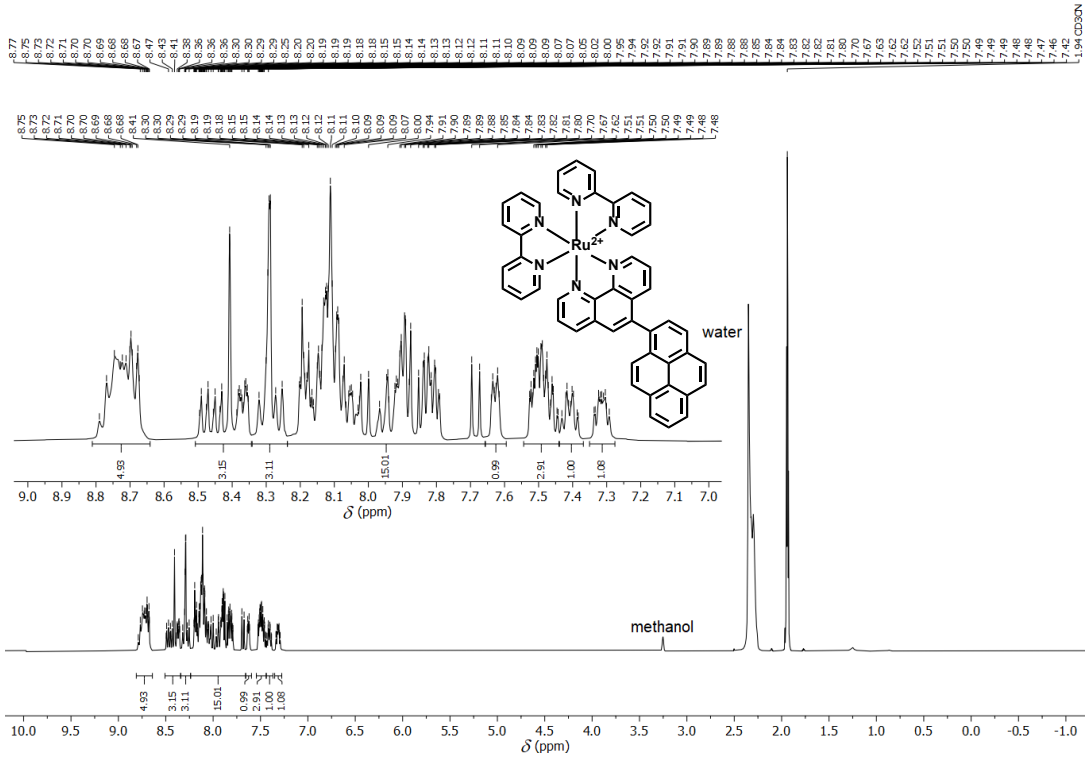

Fig. S25: ^{1}H NMR spectrum (400 MHz, CD_3CN) of RubpyPy (main plot) and aromatic region on enlarged scale (inset). The signals in the aliphatic region can be assigned to the solvents used during purification.[3,19,20]

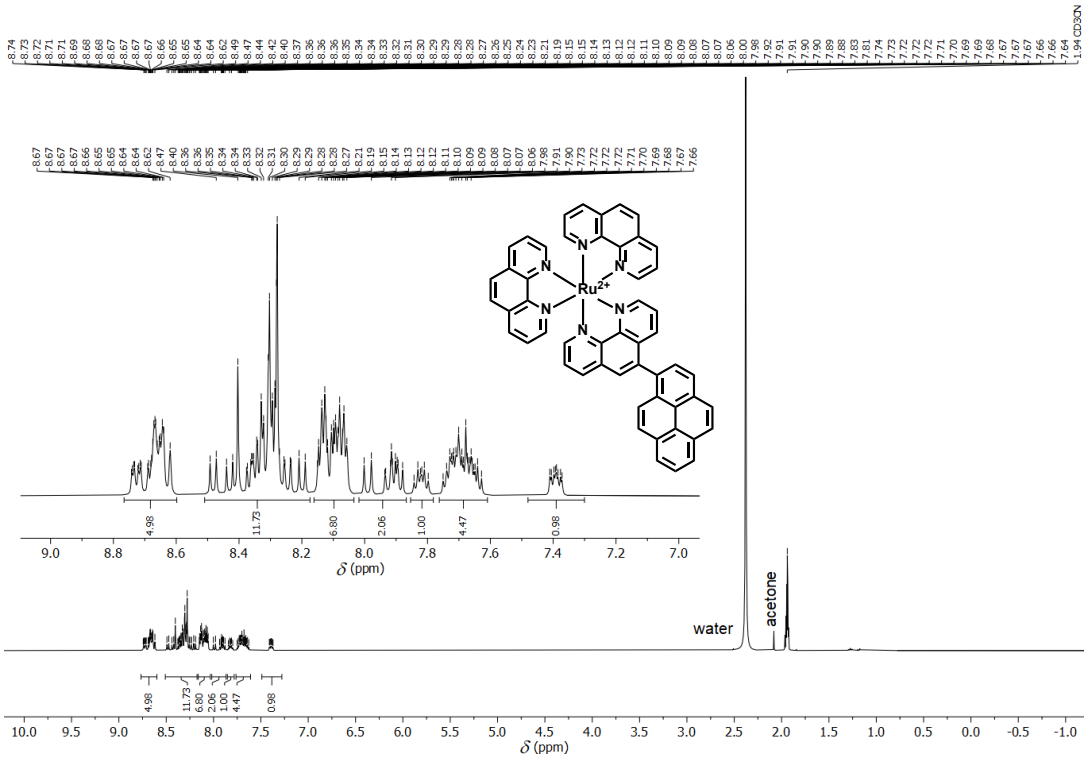

Fig. S26: ^{1}H NMR spectrum (400 MHz, CD_3CN) of RuphenPy (main plot) and aromatic region on enlarged scale (inset). The signals in the aliphatic region can be assigned to the solvents used during purification.[3,19,20]